Radiation-Induced Damage in Serine Phosphate−Insights into a Mechanism for Direct DNA Strand Breakage

Jan Lipfert,[†,‡] Jorge Llano,[‡,§] and Leif A. Eriksson*[,§,||]

Department of Quantum Chemistry, Uppsala University, Box 518, 751 20 Uppsala, Sweden, Department of Cell and Molecular Biology, Uppsala University, Box 596, 751 24 Uppsala, Sweden, and Department of Natural Sciences, Örebro University, 701 82 Örebro, Sweden

Received: November 17, 2003; In Final Form: March 26, 2004

The radiation-induced decomposition mechanisms of L-*O*-serine phosphate and the properties of the resulting radicals are explored at the hybrid Hartree−Fock−density functional theory level B3LYP, incorporating a polarized continuum model (IEF-PCM). Three different radical products were identified in earlier experimental studies, formed through deamination (radical **I**), decarboxylation plus radical exchange (radical **II**), or dephosphorylation (radical **III**) reactions, respectively. The calculated hyperfine coupling constants of the resulting radicals agree well with experimental data. The computed energetics for the two competing mechanisms resulting from electron capture, radicals **I** and **III**, show that the deamination reaction is barrierless, whereas the dephosphorylation reaction requires an initial electronic redistribution and formation of a phosphoranyl radical with trigonal bipyramidal geometry. From this, the dephosphorylation reaction has to overcome a barrier of approximately 26 kcal/mol, which explains the predominance of radical **I** over radical **III** in the experimental measurements. For radical **II**, the initial decarboxylation step resulting from electron loss was explored and found to proceed without barriers. The results of the current study have implications for radiation-induced damage of amino acids. In addition, serine phosphate is a model of a DNA sugar−phosphate fragment, and thus we may obtain new insights into a possible mechanism for cleavage of the phosphate ester bond of the DNA backbone leading to strand break.

Introduction

The DNA molecule is the most sensitive biologically essential target of ionizing radiation.[1] The mechanisms involved in radiation damage to DNA are often complex and largely originate from ionizations and free radical reactions, including radicals formed in parts of DNA directly and OH radicals generated by absorption of radiation in the surrounding aqueous medium. In addition, much attention has recently been given to the direct effects of low-energy electrons (LEE).[2] Despite their importance, many details still remain for a full understanding of the damage processes of DNA, and their implications in the form of altered bases, altered sugar moieties, release of unaltered bases, DNA−DNA or DNA−protein cross-links, or DNA strand breaks.

A DNA strand break involves the cleavage of the phosphate ester bond and can be single (on one of the strands) or double (on both strands). In general, one differentiates between two kinds of strand breaks: (a) direct strand break obtained by straight cleavage of the phosphate bond, and (b) strand break following a chemical modification of the nucleobase[3] or the deoxyribose.[4] Apart from the cleavage of the phosphate ester bond, no alterations of the phosphate moiety as such have been reported in experimental studies on full DNA samples or DNA oligomers.[5−7] Despite the fact that phosphate-centered radicals readily can be detected using EPR or ENDOR spectroscopy on irradiated model systems, the existence of phosphate-centered radicals in DNA ($ROPO_2^{-\bullet}$) was only recently confirmed, in yields of less than 0.2%.[8] These were attributed to local backbone uptake of nonsolvated low-energy electrons. Irradiation of DNA primarily leads to ionization of the aromatic bases, whose chemical behavior is fairly well understood,[1,9−12] and there is experimental evidence that primary ionic sites on the DNA molecule can lead to strand break.[13] However, the mechanisms by which the base damages are transferred to the sugar−phosphate region and how subsequent breakages of the sugar−phosphate bonds occur are still largely unknown.

On the basis of photoionization studies of organic phosphates, a proposal has been made[14] that, in the case of direct ionization of the phosphate group, the subsequent chain breakage proceeds via a "C4′-mechanism", very similar to that suggested for OH-radical-induced chain breakage.[6,15] Ionization of the phosphate group is followed by intramolecular hydrogen abstraction by the phosphatido radical from the C4′ (or possibly C5′) position, whereafter the phosphate anion is eliminated heterolytically from the C4′-radical.[14] However, to the best of our knowledge, this mechanism has not been verified on larger model systems such as oligomers or full DNA samples. For the action of local LEE, a mechanistic proposal has been put forth by Sevilla et al.,[8] based on localization of the attached electron at the phosphate group, followed by rupture on either side of the C3′−O−P bond to give a sugar- (C3′) or phosphate-centered radical, respectively.

Both the experimental difficulties in performing and interpreting the results of work on full DNA and the computational limitations on the size of a molecule that can be investigated at high accuracy have created the need to work with small model systems. One such system employed in radiation experiments aimed at obtaining a deeper understanding of the direct strand break mechanism is serine phosphate (SP), which has led to

* Corresponding author. E-mail: leif.eriksson@nat.oru.se.
† Currently at the Department of Physics, Stanford University.
‡ Department of Quantum Chemistry, Uppsala University.
§ Department of Cell and Molecular Biology, Uppsala University.
|| Department of Science, Örebro University.

10.1021/jp037499e CCC: $27.50
Published on Web 05/18/2004

SCHEME 1: Proposed Pathway for Formation of Radical I in Irradiated Serine Phosphate

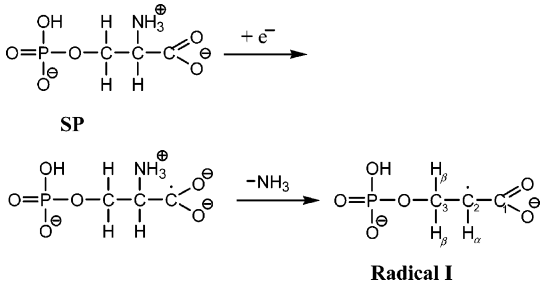

the identification of several radicals and the proposal of possible reaction pathways. Despite its small size, serine phosphate displays certain key features that are also found in the DNA strand, namely the phosphate group, the phosphate ester bond, and a carboxyl group that acts as an effective electron scavenger comparable to the nucleobases in DNA.

The work reported herein primarily refers to the experimental work by Sanderud and Sagstuen,[16] who irradiated nondeuterated and partially deuterated single crystals of L-*O*-serine phosphate at 280 K and recorded EPR, ENDOR, and field-swept ENDOR (FSE) spectra. They were able to identify three different radical species, to record their hyperfine coupling spectra, and to propose possible reaction pathways leading to their formation.

For the major radical, referred to as radical **I**, three proton resonance lines were observed. One of these displayed the characteristics of an α-proton, and the other two were of *β*-type. None of the protons were exchanged for deuterons in the partially deuterated sample. On the basis of the observed spectrum, radical **I** was assigned to be the deamination product resulting from dissociative electron capture, as outlined in Scheme 1.

The spectral lines of radical **I** disappear upon storage at room temperature, whereby radical **II** becomes the dominant species. The observed couplings for this radical were assigned to two protons and ^{14}N. One of the proton couplings is of α-type and stems from a nonexchangeable proton. The other one originates from an exchangeable proton and must therefore stem from one of the amino protons. A third proton hyperfine coupling tensor of *β*-type was observed but could not be completely determined. On the basis of the observations, radical **II** was proposed to be formed after radiation-induced electron emission, as outlined in Scheme 2. The primary oxidation causes decarboxylation, and subsequent radical exchange with a neighboring serine phosphate molecule leads to a carbon-centered radical and a nonparamagnetic species.

The remaining two proton couplings observed in the experiments were of α-type and ascribed to the minor radiation product, radical **III**. They are both nonexchangeable and their spectral similarities suggest that they are connected to the same carbon atom. Through indirect observations, the coupling of a *β*-proton could also be determined. Radical **III** was proposed to be the product resulting from loss of the phosphate group, in a mechanism initiated by electron capture followed by formation of a phosphoranyl radical intermediate that decayed (dephosphorylated) prior to detection. The proposed pathway is outlined in Scheme 3. No phosphate radical was observed in the experiments, suggesting that cleavage of the phosphate ester bond takes place at the C−O bond.

In earlier work on simple alkyl phosphate esters, three major radical species have been found to occur in the phosphate region following electron uptake.[17] Alkyl radicals (similar to radical **III**) are usually produced in the highest yields, through cleavage of the R−O bond. Alternative forms of dissociative electron

SCHEME 2: Proposed Pathway for Formation of Radical II in Irradiated Serine Phosphate[a]

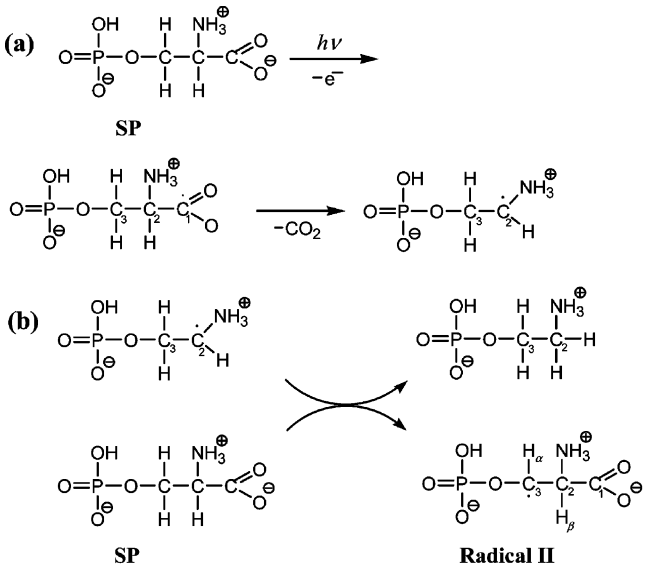

[a] (a) Photoinduced electron loss and subsequent decarboxylation. (b) Radical exchange.

SCHEME 3: Proposed Pathway for Formation of Radical III in Irradiated Serine Phosphate

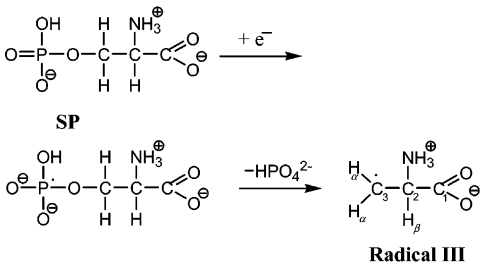

capture lead to the formation of phosphoryl radicals, $PO_3^{2-\bullet}$, and phosphoranyl radicals, $PO_4^{3-\bullet}$, that differ in the cleavage site of the phosphate ester R−O−P bond. The latter radical typically occurs in trialkyl phosphate esters.

Several model systems have been used to explore the influence of different substituents on the alkyl phosphate derivatives upon release of phosphate or phosphate-centered radicals, such as sodium or potassium salts of glucose, glycerol, or ribose phosphates.[18,19] Studies have also been conducted on related compounds such as *O*-phosphorylethanolamine (PEA), which lacks the carboxyl group of SP,[20] and aminoethyl hydrogen sulfate (AES), in which the phosphorus atom of PEA is replaced by the more electronegative sulfur.[21]

Several studies have also been performed on the parent compound serine, at temperatures ranging from 4 K (liquid helium) to room temperature.[22−25] The product distribution and possible mechanisms differ, depending on temperature and other experimental conditions, but many similarities to the SP systems can be observed. Reduction and subsequent protonation leads to a carboxyl-centered radical that undergoes elimination of the amine group by heating, whereas oxidation was found to lead to decarboxylation. Deamination and radical exchange with a nonreacted serine has been proposed to lead to the formation of the equivalence of radical **II**, whereas also a radical exchange product dehydrogenated at the amino carbon has been proposed. In addition, the oxidation product (decarboxylated radical) has been suggested to be involved in radical exchange reactions, giving the radical **II** equivalence of serine. Finally, a very

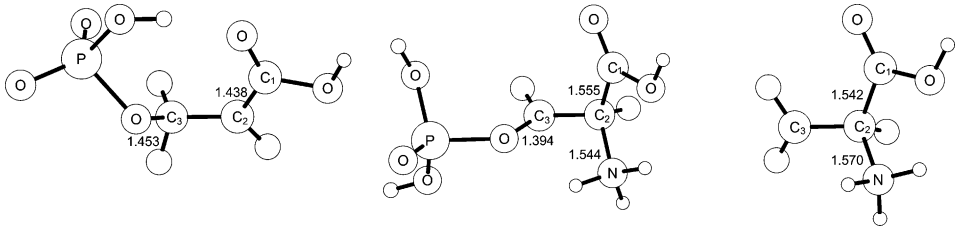

I **II** **III**

Figure 1. Optimized structures of radicals **I**, **II**, and **III** at the B3LYP/LanL2DZ level (distances in Å).

unstable radical identified as occurring due to loss of the hydroxylic hydrogen has been detected.

In the current work, we have investigated the possible reactions and products in irradiated serine phosphate by means of computational tools, as a complement to the experimental studies. During the past decade, quantum chemical methodology based on density functional theory (DFT) has emerged as an accurate setting for the study of radicals and radical properties,[26] especially since the use of more sophisticated ab initio approaches such as coupled cluster (CC) or quadratic configuration interaction (QCI) methods place very high demands on the computational resources. DFT, on the other hand, represents a reasonable compromise between good accuracy and the size of the model systems that can be explored.

Methodology

The geometries of the different systems were optimized at the hybrid Hartee−Fock−density functional theory level B3LYP,[27−29] in conjunction with the double-ζ basis sets LanL2DZ and 6-31G(d). Frequency calculations were performed at the same level of theory, to confirm the correct nature of the stationary points. It was concluded that the two basis sets produced nearly identical geometries for all systems studied.

Single point calculations of the isotropic and anisotropic radical hyperfine coupling constants (HFCCs) were computed on the optimized product structures, at the B3LYP/6-311G(2df,p) and B3LYP/6-311+G(2df,p) levels, in vacuo and embedded in a dielectric continuum (IEF-PCM method[30]) with dielectric constants $\epsilon = 4$ and $\epsilon = 78.39$. These will mimic the interior of a biochemical molecule (e.g., a protein) and bulk water, respectively. Since both the inclusion of diffuse functions as well as dielectric continuum had very little effect, these are not included in the HFCC data reported below. The suitability of these basis sets for computing radical properties and reactions have been thoroughly investigated.[31,32]

The reactions as outlined in Schemes 1−3 were investigated at the same levels as mentioned above. In the case of radicals **II** and **III**, an additional water molecule or a hydronium ion was added to stabilize the complexes in different stages of the reactions. Due to convergence difficulties in the in vacuo optimizations on the zwitterionic structures (amino group protonated, phosphate and carboxylate groups deprotonated), neutral models were utilized with the amino group as NH_2 and the phosphate and carboxylate protonated. In addition, cationic systems in which the amino group was protonated were also explored. The latter models were found to produce radical HFCCs in much better agreement with experimental data than the neutral system, confirming that in the crystal the amino group is protonated.

All calculations were performed using the Gaussian 94 and Gaussian 98 program packages.[33,34] Atomic labeling used in the text and tables throughout refers to the corresponding Schemes 1−3.

TABLE 1: Isotropic and Anisotropic Components (MHz) of the Hyperfine Coupling Tensor of Radical I, Calculated at the B3LYP/6-311G(2df,p) Level

atom	A_{iso}	T_{xx}	T_{yy}	T_{zz}
α-H (calcd)	−43.1	28.2	−1.2	−29.5
α-H (exp[a])	−54.2	32.3	3.3	−29.0
β-H1 (calcd)	105.6	8.7	−2.4	−6.3
β-H1 (exp[a])	104.3	7.2	−2.0	−5.3
β-H2 (calcd)	57.8	8.3	−3.6	−4.7
β-H2 (exp[a])	57.4	8.1	−3.9	−4.2

[a] Reference 16.

Results and Discussion

A. Radical Hyperfine Structures. Radical **I** is the deamination product of serine phosphate after electron capture, and thus a radical anion (cf. Scheme 1). The central carbon atom C2 is the proposed radical site, and is in the calculations given a value for the unpaired spin of 0.71. Some unpaired spin is also found on the carbonylic oxygen of the carboxyl group (0.18), which can be explained by the π-character of the SOMO on C2 that interacts with the conjugated system of the carboxyl group.

In Figure 1 we show the optimized structure of radical **I**, and in Table 1 we list the HFCCs of the α- and β-protons. The very near planarity of the C1−C2 fragment is in agreement with the experimental data,[16] and we note the formation of an internal hydrogen bond between the phosphate and carboxylic group. The HFCC of the α-hydrogen is in good agreement with the experimental data; the discrepancy between theory and experiment for the isotropic value can be traced back to the angle between the C2−H_α bond and the C2 SOMO, which can be affected by, for example, an incomplete sp^2 hybridization on C2 or a change in out-of-plane angle caused by crystal packing effects or explicit hydrogen bonds. The anisotropic couplings of α-protons are usually very accurately reproduced. For the two β-protons, a search of the dihedral space was required. Since these HFCCs arise as a result of hyperconjugation interaction between the π-type SOMO on C2 and the two C−H_β bonds, the induced isotropic hyperfine constants on these will be very sensitive to the amount of overlap with the SOMO. The structure with best agreement to the experimental data was found for dihedral angles with the SOMO of −1.7° and 117.2°, respectively. Two different sets of values for the dihedrals were proposed in the experimental study,[16] 13.3° and 133.3°, or 6.7° and 141.6°, respectively. Both of these sets were tested in the current work, but none of them yielded reasonable HFFCs for the β-protons.

Radical **II** occurs after ionization, decarboxylation, and subsequent radical exchange (cf. Scheme 2) and is suggested to be deprotonated at the C3 position. From the experimental spectra, the HFCCs of three protons (one exchangeable) and one nitrogen could be determined. For one of the protons, suggested to belong to a γ-hydrogen of the amine group, the

TABLE 2: Isotropic and Anisotropic Components (MHz) of the Hyperfine Coupling Tensor of Radical II, Calculated at the B3LYP/6-311G(2df,p) Level

atom	A_{iso}	T_{xx}	T_{yy}	T_{zz}
α-H (calcd)	−53.3	−36.1	−1.4	37.5
α-H (exp[a])	−51.0	−34.5	3.8	30.7
β-H (calcd)	15.4	10.8	−4.0	−6.8
β-H (exp[a])	25.0	14.0	−7.0	−8.0
β-N (calcd)	12.7	2.1	−0.9	−1.2
β-N (exp[a])	15.9	2.1	−0.3	−1.8
γ-H (calcd)	1.9	4.3	−1.5	−2.8
γ-H (exp[a])	5.9	10.1	−4.1	−5.8

[a] Reference 16.

signal was, however, very weak and the hyperfine couplings are reported to be associated with "considerable uncertainty".[16]

In Table 2 we list the computed HFCCs for the atoms in question, obtained for the optimized structure **II** shown in Figure 1. The overall agreement with experimental data is again satisfactory, although there are a few comments to be made. The computed isotropic coupling of 15 MHz for the *β*-proton (bonded to C2) appears somewhat too small. As for radical **I**, we again have the problem with small changes in the dihedral angle, for example, as resulting from crystal packing effects, that would modify the value of this hyperconjugation-induced coupling.

In the experimental paper, only one *γ*-proton tensor was reported, and it is not entirely clear from the calculations which of the three amino hydrogens this belongs to. Since the amino group is fairly exposed to the crystal lattice, small changes in the dihedral angle between the amino group and the SOMO, as well as rotation about the C2−N bond, would affect these couplings. Such modifications, which cannot be taken fully into account in the current model, are not unlikely.

The radical center C3 in radical II is hypothesized to undergo incomplete hybridization. The initial tetrahedral sp^3 hybridization transforms toward a planar sp^2 structure by hydrogen abstraction. From an analysis of the unpaired spin density obtained with McConnell and Gordy-Berhard methods, the rehybridization was found to be incomplete such that the angle between the SOMO and the plane defined by C2−C3−O is 19.5°.[16] This finding is confirmed from the computed structure, where H1 is tilted out of the C3−C2−O plane by 22°. This is in line with the work of Dobbs et al.,[35,36] who found incomplete rehybridization to be fairly common in carbon-centered radicals with oxygen as nearest neighbor, and with the results of Sornes et al.,[21] who found a similar radical structure in aminoethyl hydrogen sulfate (AES).

The incomplete rehybridization leads to a contribution of the carbon 2s orbital to the SOMO causing a deviation from pure planar geometry. The population analysis from the calculations gives a spin density of 0.84 at C3 and a minor contribution to the spin density at the neighboring oxygen of 0.11.

Radical **III** is also a C3-centered radical and is proposed to result from loss of the phosphate group after dissociative electron capture. Calculations on both the amino group protonated and on the neutral species were performed, and it was concluded that the best agreement with experiments was again found for the protonated ('zwitterionic') structure. Experimentally, two α-couplings assigned to H31 and H32 and one *β*-coupling assigned to H2 were detected.

Calculations on the geometry optimized in vacuo (Figure 1) provided hyperfine properties in less satisfactory agreement with experiment, which again can be traced back to interactions with the environment not included in the model system. In this case, the calculations predict the α-carbon to be completely rehybridized into a planar sp^2 configuration. For a satisfactory agreement with the experimental data, however, a slightly nonplanar structure was required and could be obtained by tilting the two α-hydrogens out of plane by 5° (data reported in Table 3). These findings are very similar to those previously noted for, e.g., the methyl radical $\bullet CH_3$. In this case, a slight pyramidalization is also required for the isotropic HFCCs to agree with experimental data assuming a static structure;[37] an even closer agreement with experiments is obtained upon allowing the radical to undergo umbrella-type vibrations and C−H librations that are present also at very low temperatures.[38,39] Such treatment, requiring a combined DFT and molecular dynamics methodology, is however beyond the scope of the current study.

TABLE 3: Isotropic and Anisotropic Components (MHz) of the Hyperfine Coupling Tensor of Radical III, Calculated at the B3LYP/6-311G(2df,p) Level

atom	A_{iso}	T_{xx}	T_{yy}	T_{zz}
α-H1 (calcd)	−48.8	−37.3	−1.7	39.0
α-H1 (exp[a])	−47.1	−22.0	−1.5	23.6
α-H2 (calcd)	−59.3	−37.4	−1.5	38.8
α-H2 (exp[a])	−50.8	−24.6	0.5	24.2
β-H (calcd)	73.0	8.9	−2.2	−6.7
β-H (exp[a])	73.0	(13.3)	(−6.6)	(−6.6)

[a] Reference 16.

B. Reaction Mechanisms. The different reaction pathways leading to the formation of the previously identified radicals were explored at the B3LYP/6-31G(d) level, followed by single-point calculations both in vacuo and embedded in an IEF-PCM solvation model at the B3LYP/6-311+G(2df,p) level.

Formation of radical **I** involves the release of ammonia, and thus, the calculations on this system were only performed with the amino group protonated. It turned out that, upon electron capture, the system spontaneously dissociated without barrier. The final fully optimized product structure has the ammonia at an equilibrium distance from C2 of 2.7 Å (cf. Figure 2b). To validate this finding, a scan of the C2−N distance was undertaken from 1.55 to 3 Å, allowing for the system to relax (optimize) in each step. Again, a strictly exothermic dissociation reaction without barrier was observed. At the IEF-PCM/B3LYP/6-311+G(2df,p) level, the electron capture lowers the energy (before nuclear rearrangement) by 27.4 kcal/mol, and the dissociated complex shown in Figure 2 lies another 44.7 kcal/mol lower in energy.

A strongly exothermic and barrierless reaction is in line with the experimental observation by Sanderud and Sagstuen[16] that radical **I** is the major species after irradiation. An analysis of the distribution of the unpaired spin after electron capture but before nuclear rearrangement reveals that the spin is delocalized over the entire molecule, including a large fraction (0.50) on

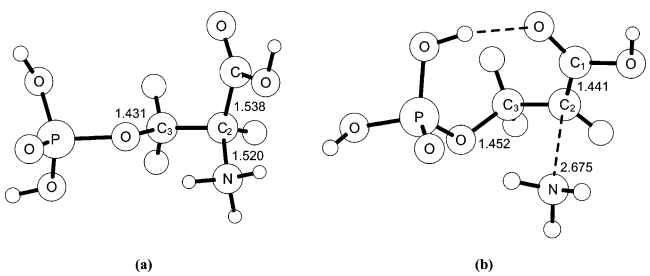

Figure 2. B3LYP/6-31G(d)-optimized structure of the protonated form of serine phosphate (distances in Å): (a) prior to electron capture and (b) after dissociative electron capture and deamination.

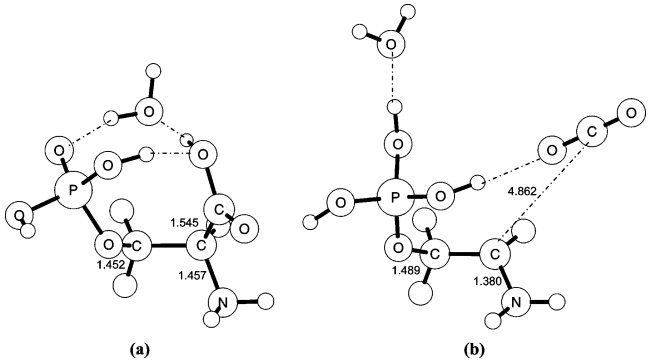

Figure 3. Optimized structure of serine phosphate and water (distances in Å): (a) prior to electron emission (B3LYP/6-31G(d) level) and (b) after dissociative electron emission and decarboxylation (HF/6-31G(d) level).

the phosphorus. The components on the other atoms are: C1, 0.74; C2, 0.34; C3, −0.34; and N, −0.31. The large component of unpaired spin on the phosphorus has implications for the possibility for formation of radical **III**, as discussed below. After fragmentation, the main component of the unpaired spin is located at the radical center C2 (0.69).

For radicals **II** and **III**, severe convergence problems were found when working with the zwitterionic (protonated) forms, and thus only the neutral conformations were employed. Radical **II** occurs after electron loss, decarboxylation, and subsequent radical exchange with another serine phosphate, which thereby becomes radical **II**, as outlined in Scheme 2. In the current study, only the first step of the sequence was investigated, i.e., the primary radiation damage leading to decarboxylation. To have a more realistic environment, an explicit water molecule was furthermore added to the system, as depicted in Figure 3a, where we show the fully optimized reactant complex.

Subsequent attempts to locate a transition state for decarboxylation were unsuccessful, just as in the case of the deamination reaction leading to radical **I**. Instead, the decarboxylation reaction also appears to be a barrierless process immediately following electron loss. In the optimizations, frequent proton-transfer back and forth between the initial radical center on C2 and the water molecule were observed, indicating the importance of subsequent protonation/hydrogenation from a second SP molecule to form the closed-shell species.

In further optimizations at the B3LYP/6-31G(d) level, the phosphate group dissociated from the remaining fragment. Attempts were therefore made to localize transition states and product complexes at the HF/6-31G(d) level of theory, since HF theory is known to provide much more corrugated energy surfaces (high barriers, stable products). However, no stable transition structures could be found for the decarboxylation reaction, which instead proceeded spontaneously. A product complex could however be obtained at the HF/6-31G(d) level, depicted in Figure 3b. This lies ca. 18 kcal/mol below the ionized initial reactant complex at the IEF-PCM//B3LYP/6-311+G(2df,p) level.

Although these calculations are far from conclusive, they do reveal that decarboxylation occurs very readily after electron loss and that the remaining system is very prone to accept a proton or hydrogen atom from its surroundings. Crystal packing may well prevent the second fragmentation (dephosphorylation) from occurring as rapidly as in the vacuum calculations, giving sufficient time for radical exchange with a neighboring molecule.

Radical **III** is formed through dissociative electron capture (Scheme 3) and is a competing mechanism to the deamination reaction leading to radical **I**. On the basis of comparisons with the reactions observed in dialkyl and dihydroxyalkyl phosphates,[5,17,19,20] it was concluded that the system must undergo an electronic reorganization such that an unstable phosphoranyl radical intermediate is formed prior to fragmentation.[16] Since no phosphoranyl radical could be detected in the experiments on serine phosphate, it was furthermore speculated that this would decay prior to observation.

In the calculations, we were able to optimize an initial complex, a phosphoranyl anion intermediate, a transition state, and the final product; in Figure 4 we show the B3LYP/6-31G(d)-optimized structures. Note that due to convergence difficulties these calculations were also made on the "neutral" model. Since the starting system as such is identical to that spontaneously leading to radical **I**, we included a hydronium ion bonded to the phosphate group in order to pull the electron toward the phosphate moiety. This also has the advantage of making the total system charge neutral after electron capture. It should be noted though, that the hydronium ion readily donates one of the protons to the negatively charged oxygen on the phosphate group. The energies of the reactant complex with hydronium ion and that in which proton transfer has occurred are, however, very similar; in aqueous solution the hydronium ion system is in fact the more stable of the two. For consistency, we show in Figure 4 the sequence optimized in vacuo, in which proton transfer has occurred.

In the course of the reaction, the unpaired spin is moving around significantly. In the reactant complex prior to nuclear relaxation we have a considerable excess of spin on the phosphorus (1.83), as well as significant unpaired spin on the other carbons in the molecule (−0.10, 0.30, and −0.65 on C1, C2, and C3, respectively). Relaxation of the geometry and formation of the phosphoranyl radical localizes the unpaired spin to the phosphorus atom (0.74). In the transition state the spin starts moving away from the phosphorus (0.59), and in the product complex it is completely transferred to the radical center C3.

The formation of a phosphoranyl anion intermediate is also clearly seen on the structural parameters of the phosphate group. In the reactant and product complexes, the phosphorus has a local tetrahedral structure, with O−P−O angles between 101° and 117°. The deviations from perfect tetrahedron depend on the protonation state of the oxygen atom in question, plus the influence of the hydrogen bond to water. In the phosphoranyl anion, on the other hand, the phosphorus attains a near trigonal bipyramidal geometry, with the O−P−O angle between the two axial oxygens being 146° and the angles from the axial to the equatorial oxygens being just above 90°. The lone electron pair occupies one of the equatorial positions. In the transition structure, the various angles are essentially halfway between those of the trigonal bipyramidal and tetrahedral structures.

Similarly to the system leading to radical **I**, the electron capture is exothermic, this time by 25 kcal/mol (IEF-PCM data). Allowing the system to relax to the phoshporanyl intermediate lowers the energy by an additional 17 kcal/mol. From this point the system has to overcome a barrier for the transition state of 26.5 kcal/mol to reach the dephosphorylated product ca. 36 kcal/mol below the intermediate. The energetics are displayed in Figure 5. Overall, the reaction is very exothermic, albeit within the current model system associated with a barrier that appears too high to make detection of the phosphoranyl intermediate in the spectroscopic measurements impossible. It is not unlikely that the reaction occurring in the crystalline environment is in fact assisted by favorable interactions with the surroundings, leading to a lowering of the barrier compared to the present results. The presence of a barrier as such, however, does provide

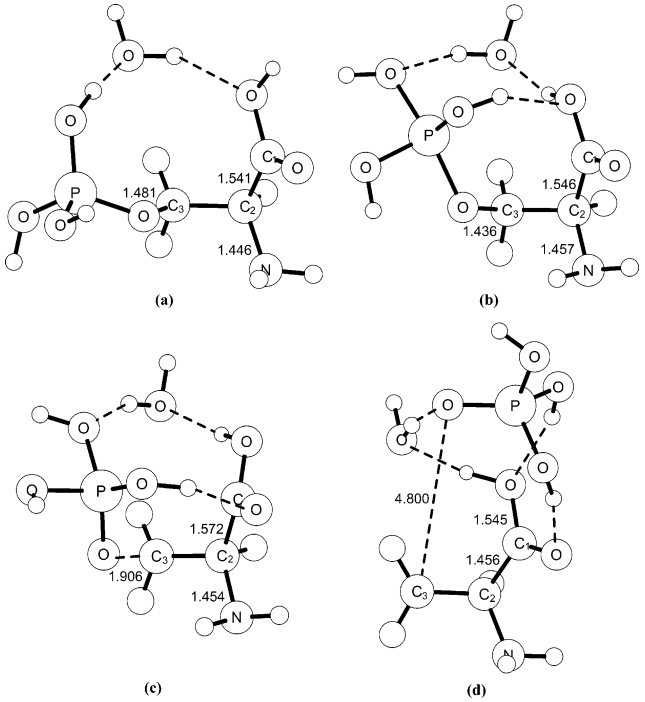

Figure 4. B3LYP/6-31G(d)-optimized structure of serine phosphate and H_3O^+ (distances in Å): (a) prior to electron capture, (b) phosphoranyl anion intermediate formed after electron uptake, (c) transition state for cleavage of the phosphate ester bond, and (d) final product complex after electron capture and dephosphorylation.

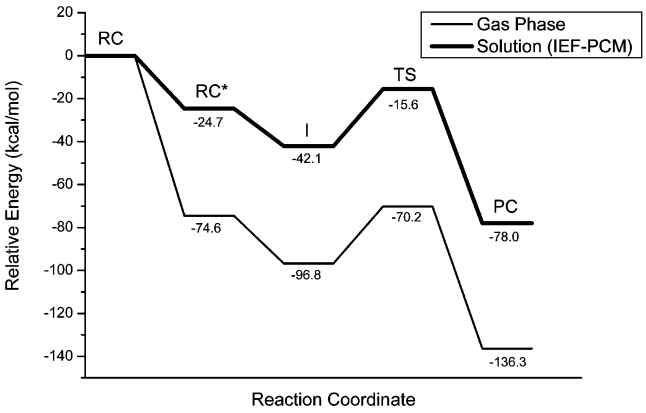

Figure 5. B3LYP/6-311+G(2df,p)//B3LYP/6-31G(d)-computed energies for formation of radical **III**. RC, reactant complex (Figure 4a); RC*, reactant complex after electron uptake (single point); I, phosphoranyl intermediate (Figure 4b), TS, transition state (Figure 4c); PC, product complex (Figure 4d).

a partial explanation for the predominance of radical **I** over radical **III** in the irradiated samples. On the basis of the observed barrier—albeit overestimated in the calculations—one may also speculate that experimental measurements performed at 4 K might make detection of this intermediate possible.

Conclusions and Possible Implications for DNA Strand Break

In the current work, we have explored the reactions and fragmentation products observed in irradiated serine phosphate by means of computational chemistry. Three different reactions were investigated: two based on electron capture and one resulting from ionization (electron loss). The computed radical hyperfine structures of the final products support the experimental findings, although we note a large sensitivity toward structural modifications resulting from crystal packing and hydrogen bonding to neighboring atoms.

Electron capture in serine phosphate results in two competing mechanisms, leading to deamination (radical **I**) or dephosphorylation (radical **III**), respectively. The deamination mechanism is strictly exothermic and proceeds without any energy barriers. This agrees well with radical **I** being the predominant product in irradiated serine phosphate, whereas radical **III** is formed in smaller fractions. The alternative mechanism, leading to radical **III**, involves an initial accumulation of the unpaired spin on the phosphorus and the formation of a trigonal bipyramidal phosphoranyl anion intermediate. The system then passes over a transition barrier for the dephosphorylation reaction, with an increase in the C−O(P) bond from 1.44 to 1.91 Å, a back-transfer of the unpaired spin to the adjacent carbon atom, and a local geometry around the phosphorus that has halfway between those of the tetrahedral and the trigonal bipyramidal structures.

The formation of the phosphoranyl intermediate is exothermic and barrierless, but the subsequent TS leading to dephosphorylation is associated with a barrier of as much as 26.5 kcal/mol. This is most likely an overestimation and is probably strongly affected by interactions with the environment. It is furthermore evident from the calculations that the environment has large impact on "steering over" the unpaired spin toward the phosphorus and thus determining whether the serine phosphate after electron capture will proceed toward radical **I** or **III**. Formation of radical **III** (corresponding to direct strand break) does not seem to depend on stereoelectronic effects other than the formation of the trigonal bipyramidal phosphoranyl anion intermediate facilitated by some external agent.

For the radical resulting from electron loss, only the initial reaction step involving decarboxylation was explored, and not the subsequent radical exchange (cf. Scheme 2). It is concluded that the decarboxylation reaction is a spontaneous process proceeding without any barriers. Indirect evidence indicates that the initial radical thereby formed is very prone to protonation or hydrogenation, which, if the hydrogen-donating group is a neighboring serine phosphate, would result in the observed radical **II**.

Since serine phosphate is only a small model system, the established reaction mechanisms are not directly applicable to the situation in irradiated DNA. However, the present work does confirm the hypothesized presence of a phosphoranyl intermediate leading to the cleavage of the phosphate ester bond in serine phosphate. It can be speculated that a similar reaction mechanism could be responsible for the cleavage of the phosphate ester bond in DNA and thus to direct strand breaks. Clearly, however, in these systems a large number of competing mechanisms are present, involving the nucleobases acting as electron sinks or pimary ionization targets, or reactions with decomposition products of irradiated water molecules (e.g. the OH radical). To draw further conclusions regarding the accessibility of the current pathways as mechanism for direct DNA strand break, more detailed theoretical investigations of irradiated ribose and deoxyribose phosphates are necessary, as well as mechanistic studies of the indirect routes proceeding via damage to the nucleobases or sugars and comparison between the energetics involved for the different schemes. Initial work along this line has been reported by Becker et al.[8] and by Li et al.[40]

Acknowledgment. The authors gratefully acknowledge the Swedish Science Research Council (VR) for financial support, the ERASMUS student exchange program, the Swedish Institute (SI), and the National Supercomputing Center (NSC) in Linköping for grants of computing time.

Supporting Information Available: B3LYP/LanL2DZ- or B3LYP/6-31G(d,p)-optimized coordinates for Figures 1−4. This

material is available free of charge via the Internet at http://pubs.acs.org.

References and Notes

(1) Von Sonntag, C.; Schuchman, H.-P. *Encyclopedia of Molecular Biology and Molecular Medicine*; VCH: Weinheim, 1996; Vol. 3.

(2) Boudaiffa, B.; Cloutier, P.; Hunting, D.; Huels, M. A.; Sanche, L. *Radiat. Res.* **2002**, *157*, 227, and references therein.

(3) Burrows, C. J.; Muller, J. G. *Chem. Rev.* **1998**, *98*, 1109.

(4) Pogozelski, W. K.; Tullius, T. D. *Chem. Rev.* **1998**, *98*, 1089.

(5) Nelson, D. J.; Symons, M. C. R.; Wyatt, J. L. *J. Chem. Soc., Faraday Trans.* **1993**, *89*, 1955.

(6) Giese, B.; Beyrich-Graf, X.; Erdmann, P.; Petretta, M.; Schwitter, U. *Chem. Biol.* **1995**, *2*, 367.

(7) Becker, D.; Razskazovskii, Y.; Sevilla, M. D. *Radiat. Res.* **1996**, *146*, 361.

(8) Becker, D.; Bryant-Friedrich, A.; Trzasko, C. A.; Sevilla, M. D. *Radiat. Res.* **2003**, *160*, 174.

(9) Berhard, W. A. *Adv. Radiat. Biol.* **1981**, *9*, 199.

(10) Close, D. M. *Magn. Res. Rev.* **1991**, *15*, 241.

(11) Hüttermann, J. In *Radical Ionic Systems: Properties in Condensed Phases*; Lund, A., Shiotani, M., Eds.; Kluwer: Dordrecht, 1991.

(12) Becker, D.; Sevilla, M. D. *Adv. Radiat. Biol.* **1993**, *17*, 121.

(13) Boon, P. J.; Cullis, P. M.; Symons, M. C. R.; Wren, B. W. *J. Chem. Soc., Perkin Trans. 2* **1984**, 1393.

(14) Steenken, S.; Goldbergerova, L. *J. Am. Chem. Soc.* **1998**, *120*, 3928.

(15) Schulte-Frohlinde, D. In *Mechanisms of DNA Damage and Repair*; Simic, M. G., Grossman, L., Upton, A. C., Eds.; Plenum: New York, 1980.

(16) Sanderud, A.; Sagstuen, E. *J. Phys. Chem.* **1996**, *100*, 9545.

(17) Nelson, D. J.; Symons, M. C. R. *J. Chem. Soc., Perkin Trans. 2* **1977**, 287.

(18) Bungum, B.; Hole, E. O.; Sagstuen, E.; Lindgren, E. *Radiat. Res.* **1994**, *139*, 194.

(19) Sanderud, A.; Sagstuen, E. *J. Chem. Soc., Faraday Trans.* **1996**, *92*, 995.

(20) Fouse, G. W.; Bernhard, W. A. *J. Chem. Phys.* **1979**, *70*, 1667.

(21) Sornes, A. R.; Sagstuen, E. *J. Phys. Chem.* **1995**, *99*, 16857.

(22) Castleman, B. W.; Moulton, G. C. *J. Chem. Phys.* **1971**, *55*, 2598.

(23) Castleman, B. W.; Moulton, G. C. *J. Chem. Phys.* **1972**, *57*, 2762.

(24) Sinclair, J. *J. Chem. Phys.* **1971**, *55*, 245.

(25) Lee, J. Y.; Box, H. C. *J. Chem. Phys.* **1973**, *59*, 2509.

(26) See, for example: *Theoretical and Computational Chemistry, Vol. 9; Theoretical Biochemistry−Processes and Properties of Biological Systems*; Eriksson, L. A., Ed.; Elsevier: Amsterdam, 2001.

(27) Becke, A. D. *J. Chem. Phys.* **1993**, *98*, 5648.

(28) Lee, C.; Yang, W.; Parr, R. G. *Phys. Rev. B* **1988**, *37*, 785.

(29) Stevens, P. J.; Devlin, F. J.; Chabalowski, C. F.; Frisch, M. J. *J. Phys. Chem.* **1994**, *98*, 11623.

(30) Tomasi, J.; Persico, M. *Chem. Rev.* **1994**, *94*, 2027.

(31) Wetmore, S. D.; Eriksson, L. A.; Boyd, R. J. In *Theoretical and Computational Chemistry, Vol. 9; Theoretical Biochemistry−Processes and Properties of Biological Systems*; Eriksson, L. A., Ed.; Elsevier: Amsterdam, 2001.

(32) Ban, F.; Gauld, J. W.; Wetmore, S. D.; Boyd, R. J. In *EPR of Free Radicals in Solids−Trends in Methods and Applications; Progress in Theoretical Chemistry and Physics*; Lund, A., Shoitani, M., Eds.; Kluwer: Dordrecht, 2003; Vol. 10.

(33) Frisch, M. J.; Trucks, G. W.; Schlegel, H. B.; Gill, P. M. W.; Johnson, B. G.; Robb, M. A.; Cheeseman, J. R.; Keith, T.; Petersson, G. A.; Montgomery, J. A.; Raghavachari, K.; Al-Laham, M. A.; Zakrzewski, V. G.; Ortiz, J. V.; Foresman, J. B.; Cioslowski, J.; Stefanov, B. B.; Nanayakkara, A.; Challacombe, M.; Peng, C. Y.; Ayala, P. Y.; Chen, W.; Wong, M. W.; Andres, J. L.; Replogle, E. S.; Gomperts, R.; Martin, R. L.; Fox, D. J.; Binkley, J. S.; Defrees, D. J.; Baker, J.; Stewart, J. P.; Head-Gordon, M.; Gonzalez, C.; Pople, J. A. *Gaussian 94*, revision B.2; Gaussian, Inc.: Pittsburgh, PA, 1995.

(34) Frisch, M. J.; Trucks, G. W.; Schlegel, H. B.; Scuseria, G. E.; Robb, M. A.; Cheeseman, J. R.; Zakrzewski, V. G.; Montgomery, J. A., Jr.; Stratmann, R. E.; Burant, J. C.; Dapprich, S.; Millam, J. M.; Daniels, A. D.; Kudin, K. N.; Strain, M. C.; Farkas, O.; Tomasi, J.; Barone, V.; Cossi, M.; Cammi, R.; Mennucci, B.; Pomelli, C.; Adamo, C.; Clifford, S.; Ochterski, J.; Petersson, G. A.; Ayala, P. Y.; Cui, Q.; Morokuma, K.; Malick, D. K.; Rabuck, A. D.; Raghavachari, K.; Foresman, J. B.; Cioslowski, J.; Ortiz, J. V.; Stefanov, B. B.; Liu, G.; Liashenko, A.; Piskorz, P.; Komaromi, I.; Gomperts, R.; Martin, R. L.; Fox, D. J.; Keith, T.; Al-Laham, M. A.; Peng, C. Y.; Nanayakkara, A.; Gonzalez, C.; Challacombe, M.; Gill, P. M. W.; Johnson, B. G.; Chen, W.; Wong, M. W.; Andres, J. L.; Head-Gordon, M.; Replogle, E. S.; Pople, J. A. *Gaussian 98*, revision A.7; Gaussian, Inc.: Pittsburgh, PA, 1998.

(35) Dobbs, A. J.; Gilbert, B. C.; Norman, O. C. *J. Chem. Soc. A* **1971**, 124.

(36) Dobbs, A. J.; Gilbert, B. C.; Norman, O. C. *J. Chem. Soc., Perkin Trans.* **1972**, *2*, 786.

(37) Eriksson, L. A.; Malkin, V. G.; Malkina, O. L.; Salahub, D. R. *Int. J. Quantum Chem.* **1994**, *52*, 879.

(38) Chipman, D. M. *Theor. Chim. Acta* **1992**, *82*, 93.

(39) Eriksson, L. A.; Laaksonen, A. *Recent Res. Devel. Phys. Chem.* **1988**, *2*, 369.

(40) Li, X.; Sevilla, M. D.; Sanche, L. *J. Am. Chem. Soc.* **2003**, *125*, 13668.